Title: Down-regulation of ceramide synthase-6 during epithelial-to-mesenchymal transition reduces plasma membrane fluidity and cancer cell motility

Authors: Valerie Edmond[a,b,d,¶], Florent Dufour[e,¶], Guillaume Poiroux[f,g,h,¶], Kenji Shoji[a,b,d,¶], Marine Malleter[a,b,d], Amelie Fouqué[a,b,d], Sébastien Tauzin[a,b,d], Ruth Rimokh[i], Odile Sergent[a,b], Aubin Penna[a,b,d], Aude Dupuy[j], Thierry Levade[f,g,h], Nathalie Theret[a,b], Olivier Micheau[e], Bruno Ségui[f,g,h], and Patrick Legembre[a,b,c,d,§].

[¶]*These authors contributed equally to this work.*

Affiliations:

[a]Université de Rennes-1, 2 Av. du Prof Léon Bernard, 35043 Rennes, France.

[b]INSERM UMR 1085, IRSET, 2 Av. du Prof Léon Bernard, 35043 Rennes, France.

[c]Centre Eugène Marquis, rue bataille Flandres Dunkerque, 35042 Rennes, France.

[d]Equipe Labellisée Ligue Contre Le Cancer, 2 Av. du Prof Léon Bernard, 35043 Rennes, France.

[e]INSERM UMR 866, 7 Bd Jeanne d'Arc, 21078 Dijon, France.

[f]INSERM UMR 1037, 31432 Toulouse, France.

[g]Université Toulouse III - Paul Sabatier, 118 route de Narbonne, 31062 Toulouse, France.

[h]Equipe Labellisée Ligue Contre Le Cancer, 31432 Toulouse, France.

[i]Inserm U1052, CNRS UMR 5286, Université de Lyon, Centre de recherche en cancérologie de Lyon, Centre Léon Bérard Lyon, France.

[j]INSERM U1048, Plateau Metatoul Lipidomique, 1, Av. Jean Poulhès, 31432 Toulouse, France.

[§]**Corresponding author:** Université de Rennes-1, Inserm U1085 - IRSET, 2 Av. du Prof Léon Bernard, 35043 Rennes, France. **Phone**: (+33)-223234807. Fax: (+33)-223234794. **E-mail:** patrick.legembre@inserm.fr

Running title: Ceramide synthesis hampers cell migration

Abstract

Epithelial-to-mesenchymal transition (EMT) promotes cell motility, which is important for the metastasis of malignant cells, and blocks CD95-mediated apoptotic signaling triggered by immune cells and chemotherapeutic regimens. CD95L, the cognate ligand of CD95, can be cleaved by metalloproteases and released as a soluble molecule (cl-CD95L). Unlike transmembrane CD95L, cl-CD95L does not induce apoptosis but triggers cell motility. Electron paramagnetic resonance was used to show that EMT and cl-CD95L treatment both led to augmentation of plasma membrane fluidity that was instrumental in inducing cell migration. Compaction of the plasma membrane is modulated, among other factors, by the ratio of certain lipids such as sphingolipids in the membrane. An integrative analysis of gene expression in NCI tumor cell lines revealed that expression of ceramide synthase-6 (CerS6) decreased during EMT. Furthermore, pharmacological and genetic approaches established that modulation of CerS6 expression/activity in cancer cells altered the level of C16-ceramide, which in turn influenced plasma membrane fluidity and cell motility. Therefore, this study identifies *CerS6* as a novel EMT-regulated gene that plays a pivotal role in the regulation of cell migration.

Keywords: Ceramide, EMT, Fas, Fluidity, Ceramide synthase, Migration.

Introduction

CD95L (also known as FasL) is a transmembrane ligand that binds to the so-called death receptor CD95 (also known as Fas/APO1). Metalloproteases can cleave CD95L to produce the soluble ligand cl-CD95L. While transmembrane CD95L is a potent apoptosis inducer that participates in immune surveillance and tolerance (see review [33]), cl-CD95L cannot induce apoptosis, but instead triggers the motility of cancer cells and activated T lymphocytes [12, 15, 35] and aggravates inflammation [23, 35]. Binding of transmembrane CD95L to CD95 leads to formation of the death-inducing signaling complex (DISC), which contains the Fas-associated via death domain (FADD) adaptor protein and caspases -8 and -10 [14]. This complex plays a pivotal role in the initiation of apoptotic signaling. Cells can be classified as type I or type II according to the efficiency with which DISC forms and their reliance on the mitochondrion-driven apoptotic signal to implement the CD95-mediated apoptotic signal [14]. We previously showed that type II cells are of epithelial lineage, whereas type I cells are mesenchymal-like [1]. Type II cells are more sensitive to the CD95-mediated apoptotic signal than type I cells; therefore, it was concluded that cancer cells undergoing epithelial-to-mesenchymal transition (EMT) reprogram their apoptotic machinery to resist CD95-mediated cell death [1]. These findings encouraged us to investigate whether EMT alters the cellular response to cl-CD95L, i.e., motility.

Sphingolipids (SLs) belong to a class of lipids whose members play multiple roles in eukaryotic cells. SLs are important structural components of membranes and are second messengers that regulate cell growth, differentiation, and death [10]. Ceramide (N-acyl-D-erythro-sphingosine) can be generated *via* hydrolysis of sphingomyelin by sphingomyelinases, or *via* ceramide synthase (CerS)-mediated *de novo* ceramide biosynthesis. This pathway involves acylation of sphinganine with fatty acyl-CoAs of chain lengths of C14–C26 to produce dihydroceramide. Alternatively, CerS can synthesize ceramide by the

salvage pathway through direct acylation of sphingosine, which is derived from SL catabolism [10]. Ceramide synthesis is orchestrated by six mammalian CerS proteins, each of which produces ceramides with restricted acyl chain lengths [20]. Among these proteins, ceramide synthase isoform 6 (CerS6) was most recently cloned [38]. Although most studies of ceramides have analyzed their impact on apoptotic signaling, these lipids also promote the formation of ordered liquid phases called lipid rafts, whose accumulation rigidifies the plasma membrane [29]. Ceramides form rigid ceramide-enriched domains when their N-acyl chain is longer than C12 [5, 7] and lead to an overall decrease in ordered lipid membranes in CerS2-null mice [30]. The biophysical properties of hepatocyte membranes are modified in CerS2-null mice, including increased fluidity [25], which is directly associated with changes in the SL composition. Furthermore, high plasma membrane fluidity is correlated with enhanced migratory/invasive ability of tumor cells [22, 31, 34, 40], which might be due to the enhanced deformability of these cells [22]. These observations raise the possibility that EMT alters the level of SL biosynthesis to increase membrane fluidity, which in turn promotes cell migration, a phenotypic change associated with EMT.

In this study, we demonstrate that EMT enhances CD95-mediated signaling to promote cell migration. An epithelial/mesenchymal comprehensive microarray analysis was used to show that CerS6 is differentially expressed during EMT and to provide evidence that the level of CerS6 expression controls the C16-ceramide membrane content of breast cancer cells, which in turn modulates their plasma membrane fluidity and motility.

Results

EMT and cl-CD95L-induced cell migrations are correlated with increased membrane fluidity. Using a transcriptomic analysis of 22 tumor cell lines of various histological origins [National Cancer Institute (NCI)] that respond differently to cytotoxic CD95L, we previously demonstrated that type I cells display a mesenchymal-like phenotype, whereas type II cells have an epithelial-like gene signature [1]. Cl-CD95L does not induce cell death but triggers cell motility [35]; therefore, we investigated whether EMT modifies the response of tumor cells to a CD95-driven pro-migratory cue. Using a Boyden chamber assay, cell motility was evaluated in various mesenchymal and epithelial-like breast cancer cells in the presence or absence of cl-CD95L (Fig. 1A). While mesenchymal-like cells migrated spontaneously across pore-containing membranes in the absence of cl-CD95L, epithelial cells did not (Fig. 1A). In addition, cl-CD95L treatment increased mesenchymal cell migration, but not epithelial cell migration (Fig. 1A). This suggests that CD95-mediated cell migration is blocked in the latter cells and/or promoted in the former cells.

Increased membrane fluidity can promote the invasion/motility of tumor cells [22, 31, 34, 40]; therefore, we next evaluated the membrane lipid packing densities of a large set of tumor cell lines. To this end, electron paramagnetic resonance (EPR) was used to quantify the S parameter, a biophysical parameter that is inversely correlated with membrane fluidity [2]. The S parameter was higher in epithelial tumor cells than in mesenchymal tumor cells (0.496±0.0088, n=17 versus 0.467±0.0215, n=20, $p \leq 0.001$; Fig. 1B), indicating that EMT led to membrane fluidization. Confirming this, membrane fluidity was higher in mesenchymal breast cancer cells than in epithelial breast cancer cells (0.464±0.0043, n=6 versus 0.476±0.0069 n=6, p=0.0043; Fig. 1B). In addition, the membrane fluidity of mesenchymal-like MDA-MB-231 breast tumor cells increased following cl-CD95L treatment (Fig. 1C). To

determine the role of plasma membrane fluidity in cell migration, MDA-MB-231 cells were pretreated with non-cytotoxic doses of the membrane stabilizing agent ursodeoxycholic acid (UDCA) [17] or the cyclopropyl fatty acid ester A2C, a compound that fluidifies plasma membranes [36]. Pre-incubation of MDA-MB-231 cells with UDCA slightly decreased basal membrane fluidity, although not significantly; however, this treatment abrogated the CD95-mediated increase in plasma membrane fluidity (Fig. 1C). By contrast, A2C treatment significantly enhanced both basal and CD95-induced cell membrane fluidity (Fig. 1C). Importantly, CD95-mediated migration of MDA-MB-231 cells was completely abolished by UDCA treatment but stimulated by A2C treatment (Fig. 1D). Collectively, these data indicate that plasma membrane fluidity increases during EMT and that this biophysical parameter has a pivotal function in both EMT-driven and CD95-mediated cell motility.

EMT triggers down-regulation of CerS6. Cholesterol and SLs participate in plasma membrane fluidity and compaction; therefore, we next investigated whether enzymes involved in the biosynthesis of these lipids are up- or down-regulated during EMT. To this end, a transcriptomic meta-analysis was performed using data from 22 tumor cell lines. These cell lines were epithelium-like or mesenchymal-like [26] and were previously categorized as type II and type I, respectively, based on their sensitivity to the CD95-mediated apoptotic signal [1]. Data were extracted from the NCBI Gene Expression Omnibus repository. The SAM tool (Significance Analysis of Microarrays) was used to identify 168 genes that were significantly up-regulated in type II cells and 542 genes that were significantly up-regulated in type I cells (Supporting Tables 1 and 2, respectively). Further analysis revealed that expression of *CerS6*, also known as *LASS6*, was significantly higher in type II (epithelial-like) cells than in type I (mesenchymal-like) cells. This *in silico* analysis was next validated experimentally at the mRNA (Fig. 2A). To rule out the possibility that this ceramide synthase

was only associated with the way tumor cells respond to an apoptotic inducer, we next evaluated whether CerS6 was differentially expressed between NCI cell lines showing an epithelial or mesenchymal-like gene signature [26]. An *in silico* analysis performed on tumor cell lines classified as epithelial or mesenchymal-like cells according to their expression levels of E-cadherin (CDH1)(epithelial marker) and Vimentin (mesenchymal marker) confirmed that the level of CerS6 transcripts was reduced in mesenchymal-like cancer cells as compared to their counterparts exhibiting an epithelial-like gene signature (Fig.S1). To confirm that CerS6 expression was down-regulated during EMT, we first evaluated the protein expression levels of two EMT markers, namely E-cadherin and Vimentin, in 47 NCI-60 tumor cell lines (Fig.S2A) that have previously been reported to display an Epithelial or mesenchymal-like phenotype[24]. We ranked these tumor cells based on their E-cadherin/Vimentin ratio (Fig. 2B) into three groups: i) an epithelial group with high E-cadherin expression, ii) an undefined group that either expressed equally the two markers or did not express them, and iii) a mesenchymal group with high Vimentin expression (Fig. 2B). Minor differences were found when we compared our classification with the one from Peter's group[24]. Indeed, among the 47 tumor cell lines tested, only five of them (OSCAR-5, PC3, SW620, SR and IGROV-1) showed a difference of classification between the two studies. The protein expression levels of CerS6 were significantly increased in epithelial cells as compared to mesenchymal tumor cells (Fig. 2C). This suggests that *CerS6* is a novel EMT-regulated gene, the expression of which in epithelial cells may alter the SL composition of plasma membranes.

To confirm that CerS6 expression was regulated during EMT, the level of CerS6 expression was evaluated in various well-established EMT models. Primary human mammary epithelial cells (HMECs) were used that have undergone sequential retroviral infections to express the telomerase catalytic subunit (hTERT), the large-T and small-t antigens of SV40, and the

oncogenic allele of H-Ras (H-Ras^{V12}), and have thereby been converted to aggressive tumor cells [4, 8]. This stepwise EMT cellular model system, which gives rise to mammary cells exhibiting epithelial (E-cadherin) or mesenchymal-like (vimentin) gene signatures, confirmed that CerS6 expression was extinguished during EMT (Fig. 2D). To confirm this, CerS6 expression was evaluated in the immortal human mammary epithelial cell line MCF10A and its K-Ras^{V12}-expressing counterpart. Expression of the mesenchymal marker N-cadherin (CDH-2) was higher and expression of the epithelial marker E-cadherin was lower in MCF10A-K-Ras^{V12} cells than in MCF10A cells, consistent with the former cells having undergone EMT (Fig.S2B and [19]). Interestingly, EMT triggered by K-Ras^{V12} expression was accompanied by a decrease in the protein level of CerS6 (Fig.S2B). Stimulation with TGF-β can trigger MCF10A and HMEC-TR breast epithelial cells to undergo EMT [11]. This inducible EMT model was used to establish that CerS6 expression is consistently reduced during EMT (Fig.S2C).

Breast cancer is a heterogeneous pathology, with tumors being classified into various subtypes based on their genomic and clinical features [32]. While luminal A and B tumors express epithelial markers, such as E-cadherin, basal-like cancer cells have a mesenchymal-like phenotype and express markers such as vimentin and N-cadherin [27]. Importantly, prognosis is poorer in patients with basal breast tumors than in patients with luminal breast tumors, and EMT is associated with tumor aggressiveness and an increased risk of metastatic dissemination in these patients [27]. A meta-analysis of breast cancer patients using the bc-GenExMiner tool [13] showed that *CerS6* expression was lower in basal tumors than in luminal tumors (Fig. S3). Overall, these data strongly support that *CerS6* expression is down-regulated in tumor cells undergoing EMT.

Overexpression of CerS6 in mesenchymal tumor cells decreases membrane fluidity and inhibits cell motility. To characterize the cellular function of CerS6 during EMT, CerS6 was overexpressed in two mesenchymal breast cancer cells, MDA-MB-231 and MDA-MB-468. Transduction of these cells with a CerS6-encoding retroviral vector generated stable cell populations overexpressing CerS6 (Fig. 3A). Strikingly, CerS6 overexpression did not alter the expression levels of the mesenchymal marker vimentin or the epithelial marker E-cadherin (Fig. 3A), suggesting that EMT controlled CerS6 expression but not vice versa. Lipidomic analysis using gas chromatography and mass spectrometry showed that CerS6 overexpression significantly increased the C16-ceramide contents of both cell lines (Fig. 3B). However, this increase did not alter the total ceramide content (Tables 1 and 2), indicating that a compensatory process served to ensure that the total ceramide content did not change in CerS6-overexpressing cells. Modulation of CerS6 expression will affect the acyl-CoA pool, which is required for the biosynthesis of glycerophospholipids, including phosphatidylcholine, phosphatidylinositol, phosphatidylserine and phosphatidylethanolamine; therefore, the levels of these lipids were evaluated in MDA-MB-231 cells, MDA-MB-468 cells, and their CerS6-overexpressing counterparts. CerS6 overexpression did not significantly affect the glycerophospholipid content (Tables 1 and 2). Ceramide can be metabolized to sphingomyelin, the major plasma membrane SL; therefore, sphingomyelin content was also monitored. Whereas CerS6 overexpression did not affect the total amount of sphingomyelin, the level of C16-sphingomyelin was significantly higher in CerS6-overexpressing cells than in control cells (Tables 1 and 2). These findings show that CerS6 overexpression leads to the accumulation of C16:0 ceramide, which is metabolized to more complex SLs such as C16:0 sphingomyelin. CerS6 overexpression slightly, but significantly, reduced basal membrane fluidity (Fig. 3C) and prevented cl-CD95L-induced membrane fluidization (Fig. 3C). In addition, CerS6 overexpression in these mesenchymal-like breast

cancer cells reduced basal and inhibited CD95-mediated cell motility (Fig. 3D). These findings indicate that ectopic CerS6 expression in mesenchymal-like tumor cells increases levels of C16:0 ceramide and its derivative C16:0 sphingomyelin, which in turn reduces membrane fluidity and inhibits cell motility.

Down-regulation of CerS6 in epithelial tumor cells enhances membrane fluidity and stimulates cell migration. To confirm that CerS6 reduces membrane fluidity and cell motility, a pharmacological inhibitor was used to perturb CerS6 activity in epithelial-like breast cancer cells, and the effects of this on plasma membrane fluidity and cell migration were determined. Fumonisin B_1 (FB1), a mycotoxin produced by *Fusarium moniliforme*, selectively inhibits CerS activity [37]. When the epithelial cell line MCF7 was treated with a non-cytotoxic concentration of FB1 for 48 hours, basal and CD95-induced membrane fluidity were slightly, but significantly, increased (Fig. S4A). In addition, FB1 treatment enhanced basal and CD95-mediated cell migration (Fig. S4B). To confirm these data, CerS6 expression was down-regulated in two epithelial breast cancer cells, MCF7 and T47D. These cells were transduced with lentiviruses encoding simultaneously GFP and shRNAs targeting different regions of CerS6 mRNA (shCerS6). All MCF7 cells and more than 80% of T47D cells were infected (GFP-positive) (Fig. 4A). Consistent with the FACS analyses, CerS6 expression was efficiently silenced in MCF7 cells and to a lesser extent in T47D cells following transduction with lentiviruses containing either shCerS6 (Fig. 4B). Furthermore, the reduction in CerS6 expression did not affect expression of EMT-related target genes, including E-cadherin and vimentin (Fig. 4B), confirming that *CerS6* is not an EMT master regulator gene.

Lipidomic analysis showed that down-regulation of CerS6 expression in MCF7 and T47D cells did not alter their total ceramide contents (see insets in Fig. 4C and Tables 3 and 4), whereas the level of C16:0 ceramide was significantly reduced (Fig. 4C). By contrast, down-

regulation of CerS6 expression was associated with a slight increase in the level of C18:0, C20:0, C24:0, or C24:1 ceramide, according to the cell line (Fig. 4C). CerS6 knockdown increased basal and CD95-mediated plasma membrane fluidity (Fig. 4D) and cell migration (Fig. 4E) in these epithelial cancer cells. Of note, the pro-migratory effect of cl-CD95L was less pronounced in shCerS6-treated MCF7 cells than in shCerS6-treated T47D cells (Fig. 4D). This may be because CerS6 expression was down-regulated more efficiently in MCF7 cells than in T47D cells (Fig. 4B), which led to a dramatic increase in the basal motility of MCF7 cells that might partially mask CD95-induced cell motility (Fig. 4E). Overall, these findings demonstrate that down-regulation of CerS6 expression in epithelial-like tumor cells enhances cell migration without affecting EMT.

C16-ceramide, the product of CerS6, reduces membrane fluidity and cell migration. Finally, to show that CerS6 overexpression induced cell membrane compaction and thereby inhibited cell migration, we evaluated the impact of its main lipid product, C16-ceramide. To this end, two mesenchymal breast cancer cells were incubated for 24 hours with a non-cytotoxic concentration of C16:0 ceramide (Fig. 5A) and membrane fluidity and cell motility were analyzed. While the addition of C16:0 ceramide slightly increased the basal S parameter in these cell lines (Fig. 5B), it completely inhibited the CD95-mediated increase in membrane fluidization (Fig. 5B). More importantly, basal and CD95-mediated migration of mesenchymal breast tumor cells was impaired when they were cultured in medium containing a non-cytotoxic concentration of C16-ceramide (Fig. 5C). These results indicate that exogenous C16-ceramide is adsorbed and retained in cell membranes, and confirm that an increased level of C16-ceramide, which is observed upon CerS6 overexpression, is instrumental in preventing CD95-mediated membrane fluidization and cell migration.

Discussion

EMT is a crucial process in embryonic development that can be partly phenocopied in carcinogenesis, giving rise to aggressive tumors with increased metastatic capacity. In the present study, we demonstrate that CerS6 expression is down-regulated during EMT, leading to increased plasma membrane fluidity, which in turn promotes cell migration.

Cells undergoing EMT exhibit morphological changes and increased motility, which is linked to striking reductions in expression of epithelial markers, such as E-cadherin, and enhanced expression of mesenchymal markers, such as vimentin and N-cadherin. Using pharmacological and genetic approaches, we showed that the level of CerS6 expression does not affect EMT *per se*. This seems to disagree with data from the Hakomori group showing that pharmacological inhibition of glucosylceramide synthase or the addition of one of its products, gangliotetraosylceramide (Gg4), modulates cell motility and changes the expression ratio of EMT-related genes in various cellular models, including the epithelial breast cancer cell line MCF-7 [6]. One explanation for this discrepancy is that the carbohydrate moiety complexity of Gg4 allows it to target other unidentified molecular targets and thereby exert additional effects on EMT compared to C16-ceramide and C16-sphingomyelin. In support of this hypothesis, the ganglioside GM2, whose expression is also decreased by inhibition of glucosylceramide synthase activity, does not reverse TGF-β-induced EMT of NMuMG cells, whereas Gg4 does [6]. In addition to the carbohydrate moiety, our findings provide insight into the pivotal roles played by the C16:0 fatty acid chain of ceramide and its derivatives in biological functions such as cell motility.

Okazaki and colleagues recently showed that sphingomyelin impairs CXCL12-mediated cell migration [3]. The current study shows that CerS6 overexpression is associated with an increase in the C16:0 sphingomyelin content; therefore, we cannot exclude the possibility that sphingomyelin contributes to the phenotypes observed. However, given that CD95-mediated

membrane fluidization and cell migration are inhibited by pre-incubation with exogenous C16-ceramide for a short period (60 minutes), C16-ceramide itself likely contributes to the modulation of membrane fluidity and cell motility during EMT.

Glycosphingolipids (GSLs) modulate various cell signaling pathways by regulating the activities of tyrosine kinase receptors [9, 21], and more specifically, epidermal growth factor (EGF) receptor [9]. Based on our recent findings showing that cl-CD95L induces a phosphoinositide 3-kinase (PI3K)-driven pro-migratory signaling pathway in mesenchymal breast tumor cells *via* recruitment of EGF receptor [18], we investigated whether C16-ceramide can prevent this signaling pathway. Analysis of phosphorylation at serine 473 of Akt, a hallmark of PI3K activation, demonstrated that C16-ceramide did not affect the CD95-mediated PI3K signaling pathway (Fig. S5). This indicates that C16-ceramide does not interfere with the initial steps of pro-migratory CD95-mediated cell signaling. The mechanistic link between CD95L and plasma membrane fluidization remains uncertain and requires further investigation.

Exogenous short-chain ceramides such as C2-ceramide inhibit migration of lung cancer cells in response to nicotine *via* activation of protein phosphatase 2A [39]. This previous study suggested that C2-ceramide directly affects cell migration. However, the authors did not eliminate the possibility that C2-ceramide that accumulates in the lipid bilayers of pulmonary cells is hydrolyzed by acid ceramidase to form sphingosine that enters the salvage pathway to form new ceramides through the activities of CerS such as CerS6. In this regard, it would be interesting to investigate the activity of CerS6 in pulmonary epithelial cells exposed to nicotine.

CerS6 expression was modulated in various cancer cell lines with epithelial- or mesenchymal-like gene signatures, in well-defined inducible EMT models, and also in a large panel of women affected by luminal or basal breast cancers (Fig. S3), which show an epithelial- or

mesenchymal-like gene signature, respectively [27]. Accordingly, we predict that in women with aggressive basal breast cancers in which CerS6 is not expressed, a slight increase in the level of C16-ceramide may help to reduce their elevated risk of metastatic dissemination.

Materials and Methods

Cell lines

The human cell lines derived from hematological cell lineage (Jurkat, CEM, H9, HL60, SKW6.4, K562, MOLT4, SR) were cultured in RPMI supplemented with 8% (v/v) heat-inactivated fetal calf serum (FCS) and 2 mM L-glutamine at 37°C in a 5% CO_2 incubator. All other cancer cell lines were cultured in DMEM supplemented with 8% (v/v) heat-inactivated FCS and 2 mM L-glutamine at 37°C in a 5% CO_2 incubator. The NCI-60 collection of human tumor cell lines came from Charles River Laboratories (Wilmington, MA, USA). Other cells were purchased from American Type Culture Collection (LGC Standards, Molsheim, France). The human mammary epithelial cell line MCF10A is spontaneously immortalized but not transformed. MCF10A cells infected with LXSN-K-RasV12 or an empty vector were kindly provided by Dr. B. H. Park (Baltimore, MD, USA) [16]. MCF10A cells were grown in DMEM/F12 medium supplemented with 5% horse serum, EGF (20 ng/mL), insulin (10 µg/mL), cholera toxin (100 ng/mL), and hydrocortisone (0.5 µg/mL) at 37°C in a 5% CO_2 incubator. HMECs infected with a retrovirus carrying hTERT, Ras, and AgT were kindly provided by Dr R. A. Weinberg (Cambridge, MA, USA) [4]. HMECs immortalized by hTERT and Ras were designated HMEC-TR.

In vitro motility assay

Boyden chambers contained membranes with a pore size of 8 µm (Millipore, Molsheim, France). After hydration of the membranes, mesenchymal cells (10^5 cells per chamber) or epithelial cells (3×10^5 cells per chamber) were added to the top chamber in low serum (1%)-containing medium. The bottom chamber was filled with low serum (1%)-containing medium in the presence or absence of cl-CD95L (100 ng/mL). Cells were cultured for 24 h at 37°C. To quantify migration, cells were mechanically removed from the top side of the membrane

using a cotton-tipped swab, and migrating cells from the reverse side were fixed with methanol and stained with Giemsa. For each experiment, five representative pictures were taken for each insert, then cells were lyzed and absorbance at 560 nm correlated to the amount of Giemsa stain was measured.

EPR

Membrane fluidity was determined by a spin-labeling method using EPR, as previously described [28]. Briefly, plasma membranes of living cells were labeled by incubating cells for 15 min at 37°C with 12-doxyl stearic acid (36 μg/mL), a fatty acid with a stable nitroxide radical ring at the C-12 position. Cells were then washed twice with PBS to remove excess 12-doxyl stearic acid and EPR spectra of the labeled samples were acquired at ambient temperature on a Bruker Elexsys EPR spectrometer operating at 3509.25 G center field, 20 mW microwave power, 9.86 GHz microwave frequency, 1.77 G modulation amplitude, and 100 kHz modulation frequency. Fluidity of the spin-labeled membranes was quantified by calculating the S parameter. An increase in the S parameter reflects a decrease in membrane fluidity, and vice versa.

Immunoblotting

Cells were lyzed for 30 min at 4°C in lysis buffer (25 mM HEPES pH 7.4, 1% (v/v) Triton X-100, 150 mM NaCl, and 2 mM EGTA supplemented with a mixture of protease inhibitors). Protein concentration was determined by the bicinchoninic acid method (Pierce, Rockford, IL, USA) according to the manufacturer's protocol. Proteins were resolved by 8, 10, or 12% SDS-PAGE and transferred to a nitrocellulose membrane (GE Healthcare, Buckinghamshire, UK). The membrane was blocked for 15 min with TBST (50 mM Tris, 160 mM NaCl, and 0.05% (v/v) Tween 20, pH 7.4) containing 5% (w/v) dried skimmed milk (TBSTM), and was then

incubated overnight at 4°C with the primary antibody diluted in TBSTM. The membrane was washed with TBST and was then incubated with peroxidase-labeled anti-mouse IgG1 or IgG2a (CliniSciences, Nanterre, France) for 45 min. Proteins were visualized using the enhanced chemiluminescence substrate kit (ECL RevelBlOt®, Ozyme, Saint Quentin en Yvelines, France).

Conflict of Interest

The authors declare no conflict of interest.

Acknowledgements

We are grateful to the L3 and microscopy facilities of the SFR Biosit (Université de Rennes-1, Rennes) for their technical assistance. We thank Nicole Therville and Julia Rochotte for their technical assistance. We also acknowledge the assistance of Drs. Pauline Le Faouder and Justine Bertrand-Michel from the lipidomic facilities (INSERM U1048, Toulouse, France). This work was supported by grants from the French Government managed by the French National Research Agency (ANR) and under the program "Investissements d'Avenir" with reference ANR-11-LABX-0021-01-LipSTIC Labex, INCa, ARC, Cancéropole Grand Ouest, Région Bretagne, Région Bourgogne, Rennes Métropole, Ligue Contre le Cancer (Comités d'Ille-et-Vilaine/du Morbihan/des Côtes d'Armor/du Maine et Loire et les comités du Doubs/de l'Yonne), Conseil Général d'Ille-et-Vilaine, project Membratox (grant number 32508), and the European union (FEDER).

Supplementary Information accompanies the paper on the Oncogene website (http://www.nature.com/onc).

References

1. Algeciras-Schimnich A, Pietras EM, Barnhart BC, Legembre P, Vijayan S, Holbeck SL *et al*. Two CD95 tumor classes with different sensitivities to antitumor drugs. Proc Natl Acad Sci U S A 2003; **100**: 11445-11450.

2. Alonso A, Meirelles NC, Tabak M. Effect of hydration upon the fluidity of intercellular membranes of stratum corneum: an EPR study. Biochim Biophys Acta 1995; **1237**: 6-15.

3. Asano S, Kitatani K, Taniguchi M, Hashimoto M, Zama K, Mitsutake S *et al*. Regulation of cell migration by sphingomyelin synthases: sphingomyelin in lipid rafts decreases responsiveness to signaling by the CXCL12/CXCR4 pathway. Mol Cell Biol 2012; **32**: 3242-3252.

4. Elenbaas B, Spirio L, Koerner F, Fleming MD, Zimonjic DB, Donaher JL *et al*. Human breast cancer cells generated by oncogenic transformation of primary mammary epithelial cells. Genes Dev 2001; **15**: 50-65.

5. Goni FM, Alonso A. Effects of ceramide and other simple sphingolipids on membrane lateral structure. Biochim Biophys Acta 2009; **1788**: 169-177.

6. Guan F, Handa K, Hakomori SI. Specific glycosphingolipids mediate epithelial-to-mesenchymal transition of human and mouse epithelial cell lines. Proc Natl Acad Sci U S A 2009; **106**: 7461-7466.

7. Gulbins E, Dreschers S, Wilker B, Grassme H. Ceramide, membrane rafts and infections. J Mol Med (Berl) 2004; **82**: 357-363.

8. Hahn WC, Dessain SK, Brooks MW, King JE, Elenbaas B, Sabatini DM *et al*. Enumeration of the simian virus 40 early region elements necessary for human cell transformation. Mol Cell Biol 2002; **22**: 2111-2123.

9. Hanai N, Dohi T, Nores GA, Hakomori S. A novel ganglioside, de-N-acetyl-GM3 (II3NeuNH2LacCer), acting as a strong promoter for epidermal growth factor receptor kinase and as a stimulator for cell growth. J Biol Chem 1988; **263**: 6296-6301.

10. Hannun YA, Obeid LM. Principles of bioactive lipid signalling: lessons from sphingolipids. Nat Rev Mol Cell Biol 2008; **9**: 139-150.

11. Hesling C, Fattet L, Teyre G, Jury D, Gonzalo P, Lopez J *et al*. Antagonistic regulation of EMT by TIF1gamma and Smad4 in mammary epithelial cells. EMBO Reports 2011; **12**: 665-672.

12. Hoogwater FJ, Nijkamp MW, Smakman N, Steller EJ, Emmink BL, Westendorp BF *et al*. Oncogenic K-Ras turns death receptors into metastasis-promoting receptors in human and mouse colorectal cancer cells. Gastroenterology 2010; **138**: 2357-2367.

13. Jezequel P, Frenel JS, Campion L, Guerin-Charbonnel C, Gouraud W, Ricolleau G *et al*. bc-GenExMiner 3.0: new mining module computes breast cancer gene expression correlation analyses. Database : the journal of biological databases and curation 2013; **2013**: bas060.

14. Kischkel FC, Hellbardt S, Behrmann I, Germer M, Pawlita M, Krammer PH *et al*. Cytotoxicity-dependent APO-1 (Fas/CD95)-associated proteins form a death-inducing signaling complex (DISC) with the receptor. Embo J 1995; **14**: 5579-5588.

15. Kleber S, Sancho-Martinez I, Wiestler B, Beisel A, Gieffers C, Hill O *et al*. Yes and PI3K bind CD95 to signal invasion of glioblastoma. Cancer Cell 2008; **13**: 235-248.

16. Konishi H, Karakas B, Abukhdeir AM, Lauring J, Gustin JP, Garay JP *et al*. Knock-in of mutant K-ras in nontumorigenic human epithelial cells as a new model for studying K-ras mediated transformation. Cancer Res 2007; **67**: 8460-8467.

17. Luciano L, Konitz H, Reale E. Localization of cholesterol in the colonic epithelium of the guinea pig: regional differences and functional implications. Cell and tissue research 1989; **258**: 339-347.

18. Malleter M, Tauzin S, Bessede A, Castellano R, Goubard A, Godey F *et al*. CD95L cell surface cleavage triggers a prometastatic signaling pathway in triple-negative breast cancer. Cancer Res 2013; **73**: 6711-6721.

19. Morel AP, Lievre M, Thomas C, Hinkal G, Ansieau S, Puisieux A. Generation of breast cancer stem cells through epithelial-mesenchymal transition. PLoS One 2008; **3**: e2888.

20. Mullen TD, Hannun YA, Obeid LM. Ceramide synthases at the centre of sphingolipid metabolism and biology. Biochem J 2012; **441**: 789-802.

21. Mutoh T, Tokuda A, Miyadai T, Hamaguchi M, Fujiki N. Ganglioside GM1 binds to the Trk protein and regulates receptor function. Proc Natl Acad Sci U S A 1995; **92**: 5087-5091.

22. Nakazawa I, Iwaizumi M. A role of the cancer cell membrane fluidity in the cancer metastases: an ESR study. Tohoku J Exp Med 1989; **157**: 193-198.

23. O' Reilly LA, Tai L, Lee L, Kruse EA, Grabow S, Fairlie WD *et al*. Membrane-bound Fas ligand only is essential for Fas-induced apoptosis. Nature 2009; **461**: 659-663.

24. Park SM, Gaur AB, Lengyel E, Peter ME. The miR-200 family determines the epithelial phenotype of cancer cells by targeting the E-cadherin repressors ZEB1 and ZEB2. Genes Dev 2008; **22**: 894-907.

25. Pewzner-Jung Y, Park H, Laviad EL, Silva LC, Lahiri S, Stiban J *et al*. A critical role for ceramide synthase 2 in liver homeostasis: I. alterations in lipid metabolic pathways. J Biol Chem 2010; **285**: 10902-10910.

26. Ross DT, Scherf U, Eisen MB, Perou CM, Rees C, Spellman P *et al*. Systematic variation in gene expression patterns in human cancer cell lines. Nat Genet 2000; **24**: 227-235.

27. Sarrio D, Rodriguez-Pinilla SM, Hardisson D, Cano A, Moreno-Bueno G, Palacios J. Epithelial-mesenchymal transition in breast cancer relates to the basal-like phenotype. Cancer research 2008; **68**: 989-997.

28. Sergent O, Tomasi A, Ceccarelli D, Masini A, Nohl H, Cillard P *et al*. Combination of iron overload plus ethanol and ischemia alone give rise to the same endogenous free iron pool. Biometals : an international journal on the role of metal ions in biology, biochemistry, and medicine 2005; **18**: 567-575.

29. Silva LC, de Almeida RF, Castro BM, Fedorov A, Prieto M. Ceramide-domain formation and collapse in lipid rafts: membrane reorganization by an apoptotic lipid. Biophys J 2007; **92**: 502-516.

30. Silva LC, Ben David O, Pewzner-Jung Y, Laviad EL, Stiban J, Bandyopadhyay S *et al*. Ablation of ceramide synthase 2 strongly affects biophysical properties of membranes. Journal of lipid research 2012; **53**: 430-436.

31. Sok M, Sentjurc M, Schara M, Stare J, Rott T. Cell membrane fluidity and prognosis of lung cancer. The Annals of thoracic surgery 2002; **73**: 1567-1571.

32. Sorlie T, Perou CM, Tibshirani R, Aas T, Geisler S, Johnsen H *et al*. Gene expression patterns of breast carcinomas distinguish tumor subclasses with clinical implications. Proc Natl Acad Sci U S A 2001; **98**: 10869-10874.

33. Strasser A, Jost PJ, Nagata S. The many roles of FAS receptor signaling in the immune system. Immunity 2009; **30**: 180-192.

34. Taraboletti G, Perin L, Bottazzi B, Mantovani A, Giavazzi R, Salmona M. Membrane fluidity affects tumor-cell motility, invasion and lung-colonizing potential. Int J Cancer 1989; **44**: 707-713.

35. Tauzin S, Chaigne-Delalande B, Selva E, Khadra N, Daburon S, Contin-Bordes C *et al*. The naturally processed CD95L elicits a c-yes/calcium/PI3K-driven cell migration pathway. PLoS Biol 2011; **9**: e1001090.

36. Vlasic N, Medow MS, Schwarz SM, Pritchard KA, Jr., Stemerman MB. Lipid fluidity modulates platelet aggregation and agglutination in vitro. Life sciences 1993; **53**: 1053-1060.

37. Wang E, Norred WP, Bacon CW, Riley RT, Merrill AH, Jr. Inhibition of sphingolipid biosynthesis by fumonisins. Implications for diseases associated with Fusarium moniliforme. J Biol Chem 1991; **266**: 14486-14490.

38. Weinmann A, Galle PR, Teufel A. LASS6, an additional member of the longevity assurance gene family. Int J Mol Med 2005; **16**: 905-910.

39. Xu L, Deng X. Suppression of cancer cell migration and invasion by protein phosphatase 2A through dephosphorylation of mu- and m-calpains. J Biol Chem 2006; **281**: 35567-35575.

40. Zeisig R, Koklic T, Wiesner B, Fichtner I, Sentjurc M. Increase in fluidity in the membrane of MT3 breast cancer cells correlates with enhanced cell adhesion in vitro and increased lung metastasis in NOD/SCID mice. Arch Biochem Biophys 2007; **459**: 98-106.

Figure Legends

Figure 1. Plasma membrane fluidity is a pivotal biophysical parameter modulating breast cancer cell motility. A. ***Left panel:*** Migration of the indicated epithelial and mesenchymal-like breast tumor cells was assessed using the Boyden chamber assay in the presence or absence of cl-CD95L (100 ng/mL) for 24 h. Migrating cells were stained with Giemsa. For each experiment, five images of random fields were acquired. A representative image is shown. Bars=70 μm. ***Right panel:*** Giemsa-stained cells that migrated to the lower side of the membrane were lysed and absorbance was measured at a wavelength of 560 nm. **B.** ***Upper panel***: Membrane fluidity of mesenchymal (Hs578T, MDA-MB-231, MDA-MB-468, H9, SKW6.4, U251 and Caki-1) and epithelial (MCF-7, T47D, ZR75-1, CEM, Jurkat, HCT116 and HL60) cancer cell lines was assessed using EPR. Statistical analyses were performed using the non-parametric Mann-Whitney U test (***, $p<0.001$). ***Lower panel***: Membrane fluidity was measured in epithelial (MCF-7, T47D, and ZR75-1) and mesenchymal (Hs578T, MDA-MB-231, and MDA-MB-468) breast tumor cells. Statistical analyses were performed using the non-parametric Mann-Whitney U test (**, $p<0.01$). **C.** The mesenchymal cell line MDA-MB-231 was pre-incubated with the membrane stabilizing agent UDCA (100 μM) or the fluidizing agent A2C (5 μM) for 30 min and then incubated with or without cl-CD95L (100 ng/mL) for 24 h. Membrane fluidity was quantified by EPR. Values are means ± SEM of three to five independent experiments (*, $p<0.05$). **D.** The Boyden chamber assay was used to assess the migration of MDA-MB-231 cells pre-incubated with UDCA (100 μM) or A2C (5 μM) for 30 min and then stimulated with or without cl-CD95L (100 ng/mL) for 24 h. Giemsa-stained cells that migrated to the lower side of the membrane (left panel) were lysed and absorbance at 560 nm was measured (right panel). Values

represent the means ± SEM of three independent experiments. * $p<0.05$ calculated using the two-tailed Mann-Whitney U test.

Figure 2. EMT triggers down-regulation of CerS6 expression. A. Comparative levels of CerS6 transcripts in Type I (Hs578T, MDA-MB-231, MDA-MB-468, H9, SKW6.4, U251 and Caki-1) and Type II (MCF-7, T47D, ZR75-1, CEM, Jurkat, HCT116 and HL60) cell lines using quantitative PCR. Fold change was calculated as follows: $2^{-(\text{Ct sample-Ct housekeeping gene})-(\text{Ct Mean reference set of cells-Ct housekeeping gene})}$, where the fold change in the mRNA level is relative to that in a set of four reference cell lines (Hs578T, H9, CEM, and ZR75-1). Statistical analyses were performed using the non-parametric Mann-Whitney U test (***, $p<0.001$). Values represent medians and interquartiles of three independent experiments. **B.** 47 cancer cells of the NCI-60 cell line collection were ranked according to their ratio of E-cadherin/Vimentin expression. Undefined cell lines express either both or no markers. The E-cadherin/Vimentin ratio was assessed by densitometry analysis of the data shown in Fig.S2A. **C.** Protein levels of CerS6 were quantified by densitometry analysis of data shown in Fig.S2A and compared between epithelial and mesenchymal-like tumor cells. Statistical analyses were performed using the non-parametric Mann-Whitney U test (**, $p<0.01$). Values represent medians and interquartiles. N depicts number of cells present in each lineage. **D.** Schematic representation of the successive steps of the transformation of primary HMECs infected with hTERT, small-t and large-T antigens of SV40, and H-Ras^{V12}. Cells were lyzed and 100 µg of protein was loaded per lane. Western blotting was performed with the indicated antibodies.

Figure 3. CerS6 overexpression in mesenchymal tumor cells increases the level of C16:0 ceramide, decreases plasma membrane fluidity, and inhibits cell migration. A. MDA-MB-231 or MDA-MB-468 breast cancer cells were transduced with a retroviral vector

encoding HA-tagged wild-type CerS6 (CerS6-HA) or a control vector (Mock). Indicated cells were lyzed and immunoblotting was performed. **B.** Ceramide levels were determined by mass spectrometry. Values are means ± SEM of three independent experiments. *, $p<0.05$. **C.** Indicated cells were incubated in the presence or absence of cl-CD95L (100 ng/mL) for 30 min. Membrane fluidity was assessed by EPR. Values are means ± SEM of four independent experiments. *, $p<0.05$. **D.** The Boyden chamber assay was used to assess the migration of MDA-MB-468 (left panels) and MDA-MB-231 (right panels) cells cultured with or without cl-CD95L (100 ng/mL) for 24 h. Migrating cells were stained with Giemsa. For each experiment, five images of random fields were acquired. A representative image is shown. Bars=70 μm. Giemsa-stained migrating cells were lysed and absorbance at 560 nm was recorded. Values are means ± SEM of three independent experiments (* $p<0.05$; ns, not significant).

Figure 4. Silencing of CerS6 in epithelial breast cancer cells reduces the level of C16:0 ceramide, increases plasma membrane fluidity, and promotes cell migration. A. MCF7 and T47D breast cancer cells were transduced with lentiviruses encoding scrambled or CerS6-targeting shRNA (shCerS6 #236 and #241). Infection efficiency was monitored by examining the level of GFP expression using flow cytometry. **B.** Down-regulation of CerS6 was confirmed by immunoblotting. β-actin was used as a loading control. **C.** Ceramide species were quantified by mass spectrometry in the indicated cell populations. Values are means ± SD of three independent experiments (*$p<0.05$, **$p<0.01$, ***$p<0.001$). **D.** Membrane fluidity was assessed by EPR using a spin-labeling method. **E.** Cell migration was assessed using Boyden chambers. Migrating cells were stained with Giemsa and lysed, and then

absorbance at 560 nm was recorded. Values represent means ± SEM of three independent experiments (*p<0.05).

Figure 5. Treatment of mesenchymal breast cancer cells with exogenous C16:0 ceramide reduces plasma membrane fluidity and prevents basal and CD95-mediated cell migration. A. MDA-MB-468 and MDA-MB-231 cells were treated for 24 h with the indicated concentration of C16:0 ceramide. Cell death was quantified using the MTT assay (metabolic activity). **B.** The indicated cells were pre-incubated with or without a non-cytotoxic dose (1 μM) of C16:0 ceramide (C16-Cer) for 60 min, and were then incubated with or without cl-CD95L (100 ng/mL) for 30 min. Membrane fluidity was assessed by EPR. Values are means ± SEM of four independent experiments (*, p<0.05; ns, not significant). **C.** Indicated cells were pretreated with or without C16:0 ceramide (1 μM) for 60 min and were then incubated with or without cl-CD95L (100 ng/mL) for 24 h. Cell migration was assessed by the Boyden chamber assay. Bars=70 μm. Giemsa-stained cells that migrated to the lower side of the membrane were lysed and absorbance at 560 nm was recorded. Values represent the means and SEM of three independent experiments (* p<0.05).

Table 1. Lipidomic analysis of MDA-MB-231 cells infected with mock or CerS6-HA-encoding retroviruses. Data are means ± S.E.M. of three independent experiments (**, $p<0.01$).

Lipids (nmol/mg of proteins)	MDA-MB-231 Mock	MDA-MB-231 CerS6-HA
Ceramide	**0.262** ± 0.020	**0.284** ± 0.022
Sphingomyelin	**2.93** ± 0.338	**3.32** ± 0.111
C16:0-Sphingomyelin	**1.49** ± 0.061	**1.97** ± 0.056 **
Phosphatidylcholine	**54.33** ± 4.293	**50.98** ± 6.580
Phosphatidylethanolamine	**13.06** ± 1.101	**12.92** ± 1.024
Phosphatidylserine	**1.10** ± 0.100	**1.00** ± 0.019
Phosphatidylinositol	**11.03** ± 2.798	**10.76** ± 2.121
Cholesterol	**24.79** ± 0.590	**24.66** ± 1.266
Diacylglycerol	**3.20** ± 0.374	**4.69** ± 1.833

Table 2. Lipidomic analysis of MDA-MB-468 cells infected with mock or CerS6-HA-encoding retroviruses. Data are means ± S.E.M. of three independent experiments (**, $p<0.01$).

Lipids (nmol/mg of proteins)	MDA-MB-468 Mock	MDA-MB-468 CerS6-HA
Ceramide	**0.301** ± 0.017	**0.313** ± 0.041
Sphingomyelin	**3.19** ± 0.074	**3.28** ± 0.542
C16:0-Sphingomyelin	**1.53** ± 0.076	**2.04** ± 0.034 **
Phosphatidylcholine	**40.62** ± 2.428	**49.37** ± 4.228
Phosphatidylethanolamine	**11.26** ± 0.481	**12.59** ± 1.181
Phosphatidylserine	**1.00** ± 0.058	**1.05** ± 0.103
Phosphatidylinositol	**9.50** ± 1.985	**8.04** ± 1.053
Cholesterol	**24.72** ± 3.656	**23.80** ± 0.241
Diacylglycerol	**4.24** ± 1.753	**3.60** ± 1.977

Table 3. Lipidomic analysis of MCF7 cells infected with lentiviruses encoding scrambled or CerS6-targeting shRNA. Data are means ± S.E.M. of three independent experiments (*, $p<0.05$, **, $p<0.01$).

Lipids (nmol/mg of proteins)	MCF7 Scrambled	MCF7 shCerS6#236	MCF7 shCerS6#241
Ceramide	**0.232** ± 0.049	**0.237** ± 0.027	**0.257** ± 0.023
Sphingomyelin	**3.07** ± 0.456	**5.07** ± 0.303 *	**4.27** ± 0.2 $^{p=0.05}$
C16:0-Sphingomyelin	**1.04** ± 0.09	**0.63** ± 0.039 *	**0.56** ± 0.049 **
Phosphatidylcholine	**41.69** ± 4.294	**48.76** ± 1.622	**51.70** ± 6.01
Phosphatidylethanolamine	**18.54** ± 0.813	**22.57** ± 1.64 $^{p=0.06}$	**22.26** ± 0.85 *
Phosphatidylserine	**0.917** ± 0.106	**1.091** ± 0.115	**1.013** ± 0.064
Phosphatidylinositol	**3.38** ± 0.606	**4.76** ± 0.641	**4.48** ± 0.6
Cholesterol	**23.77** ± 3.053	**23.16** ± 2.187	**24.81** ± 0.671
Diacylglycerol	**4.15** ± 2.412	**5.75** ± 3.06	**6.09** ± 3.719

Table 4. Lipidomic analysis of T47D cells infected with lentiviruses encoding scrambled or CerS6-targeting shRNA. Data are means ± S.E.M. of three independent experiments (*, $p<0.05$).

Lipids (nmol/mg of proteins)	T47D Scrambled	T47D CerS6#236	T47D CerS6#241
Ceramide	**0.646** ± 0.078	**0.416** ± 0.208	**0.626** ± 0.053
Sphingomyelin	**3.52** ± 0.739	**3.98** ± 1.396	**4.03** ± 0.969
C16:0-Sphingomyelin	**2.16** ± 0.127	**1.62** ± 0.54 $^{p=0.09}$	**2.01** ± 0.055
Phosphatidylcholine	**63.74** ± 7.666	**47.12** ± 24.968	**54.94** ± 8.386
Phosphatidylethanolamine	**23.26** ± 3.354	**17.03** ± 8.552	**21.83** ± 3.341
Phosphatidylserine	**1.117** ± 0.007	**0.768** ± 0.388	**1.237** ± 0.098
Phosphatidylinositol	**2.24** ± 0.284	**1.09** ± 0.58 $^{p=0.09}$	**1.33** ± 0.163 *
Cholesterol	**29.47** ± 2.473	**29.51** ± 2.254	**27.52** ± 0.907
Diacylglycerol	**6.68** ± 1.442	**11.08** ± 3.979	**8.9** ± 2.535

Figure 1

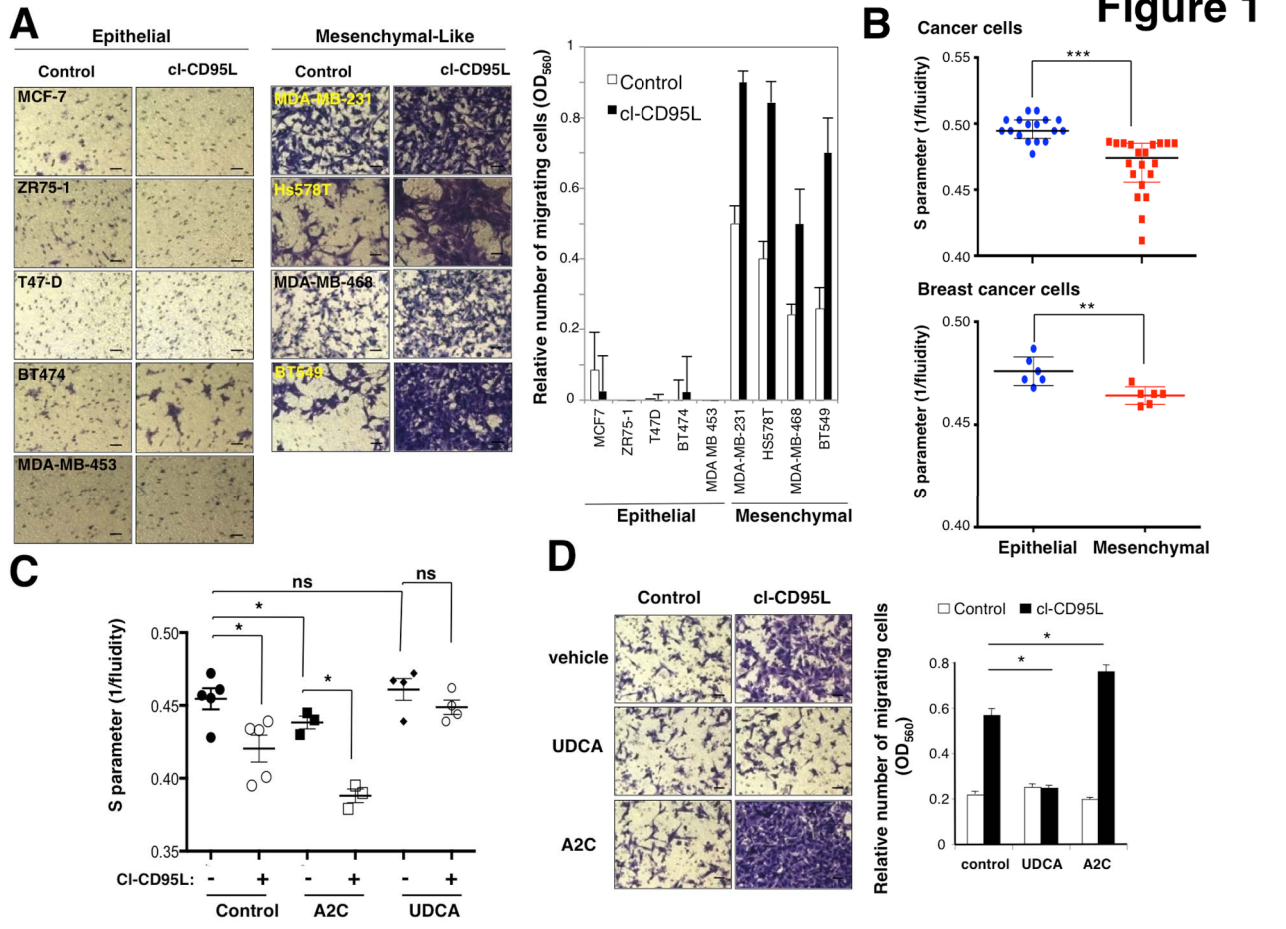
A
Epithelial
Mesenchymal-Like
Control
cl-CD95L
MCF-7
ZR75-1
T47-D
BT474
MDA-MB-453
MDA-MB-231
HS578T
MDA-MB-468
BT549
Relative number of migrating cells (OD560)
Control
cl-CD95L
MCF7
ZR75-1
T47D
BT474
MDA MB 453
MDA-MB-231
HS578T
MDA-MB-468
BT549
Epithelial
Mesenchymal
B
Cancer cells
S parameter (1/fluidity)
***
Breast cancer cells
**
Epithelial
Mesenchymal
C
S parameter (1/fluidity)
ns
ns
*
*
*
Cl-CD95L:
Control
A2C
UDCA
D
Control
cl-CD95L
vehicle
UDCA
A2C
Relative number of migrating cells (OD560)
control
UDCA
A2C

Figure 2

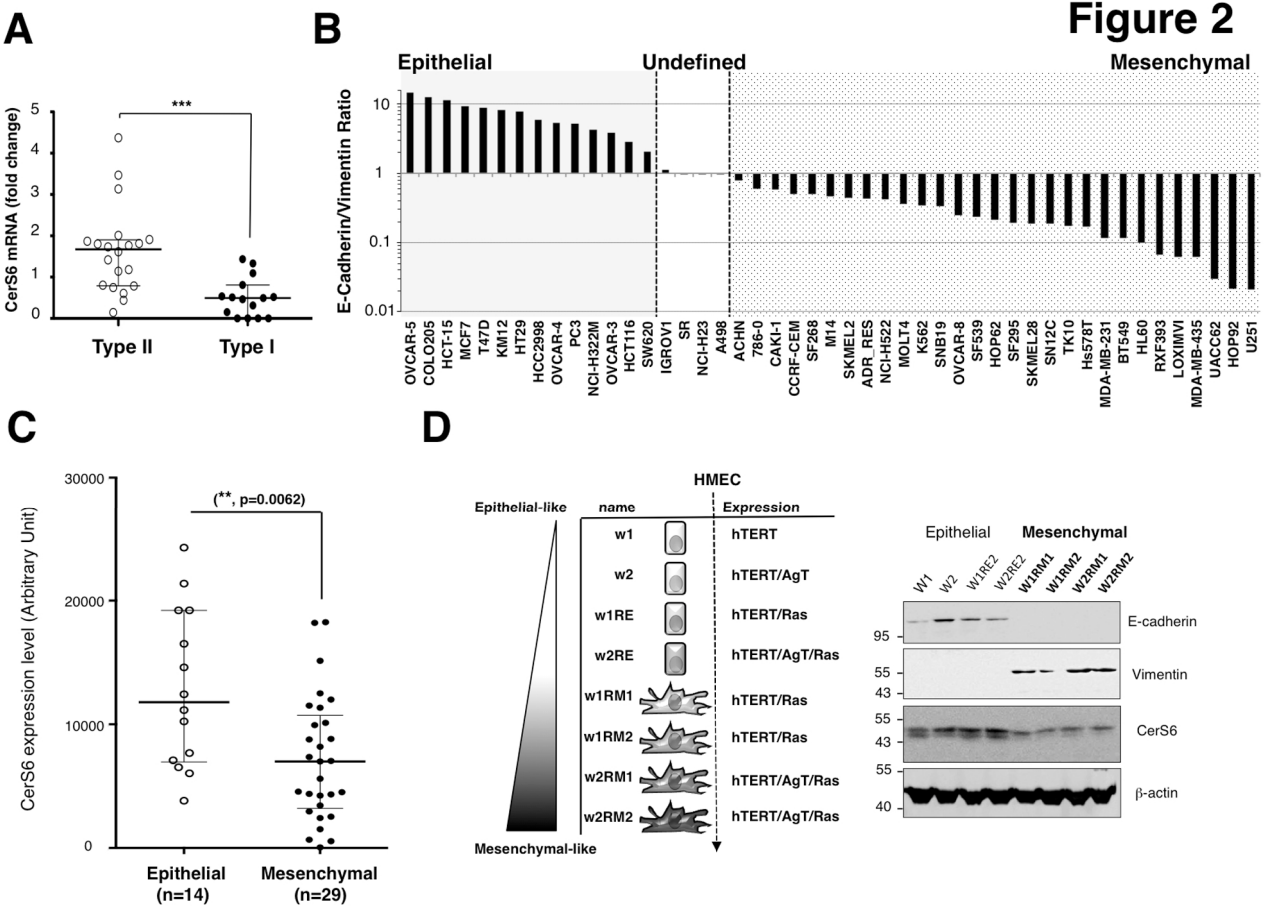
A
CerS6 mRNA (fold change)
***
Type II
Type I
B
Epithelial
Undefined
Mesenchymal
E-Cadherin/Vimentin Ratio
OVCAR-5
COLO205
HCT-15
MCF7
T47D
KM12
HT29
HCC2998
OVCAR-4
PC3
NCI-H322M
OVCAR-3
HCT116
SW620
IGROV1
SR
NCI-H23
A498
ACHN
786-0
CAKI-1
CCRF-CEM
SF268
M14
SKMEL2
ADR_RES
NCI-H522
MOLT4
K562
SNB19
OVCAR-8
SF539
HOP62
SF295
SKMEL28
SN12C
TK10
Hs578T
MDA-MB-231
BT549
HL60
RXF393
LOXIMVI
MDA-MB-435
UACC62
HOP92
U251
C
CerS6 expression level (Arbitrary Unit)
(**, p=0.0062)
Epithelial (n=14)
Mesenchymal (n=29)
D
HMEC
Epithelial-like
name
Expression
w1
hTERT
w2
hTERT/AgT
w1RE
hTERT/Ras
w2RE
hTERT/AgT/Ras
w1RM1
hTERT/Ras
w1RM2
hTERT/Ras
w2RM1
hTERT/AgT/Ras
w2RM2
hTERT/AgT/Ras
Mesenchymal-like
Epithelial
Mesenchymal
W1
W2
W1RE2
W2RE2
W1RM1
W1RM2
W2RM1
W2RM2
E-cadherin
Vimentin
CerS6
β-actin

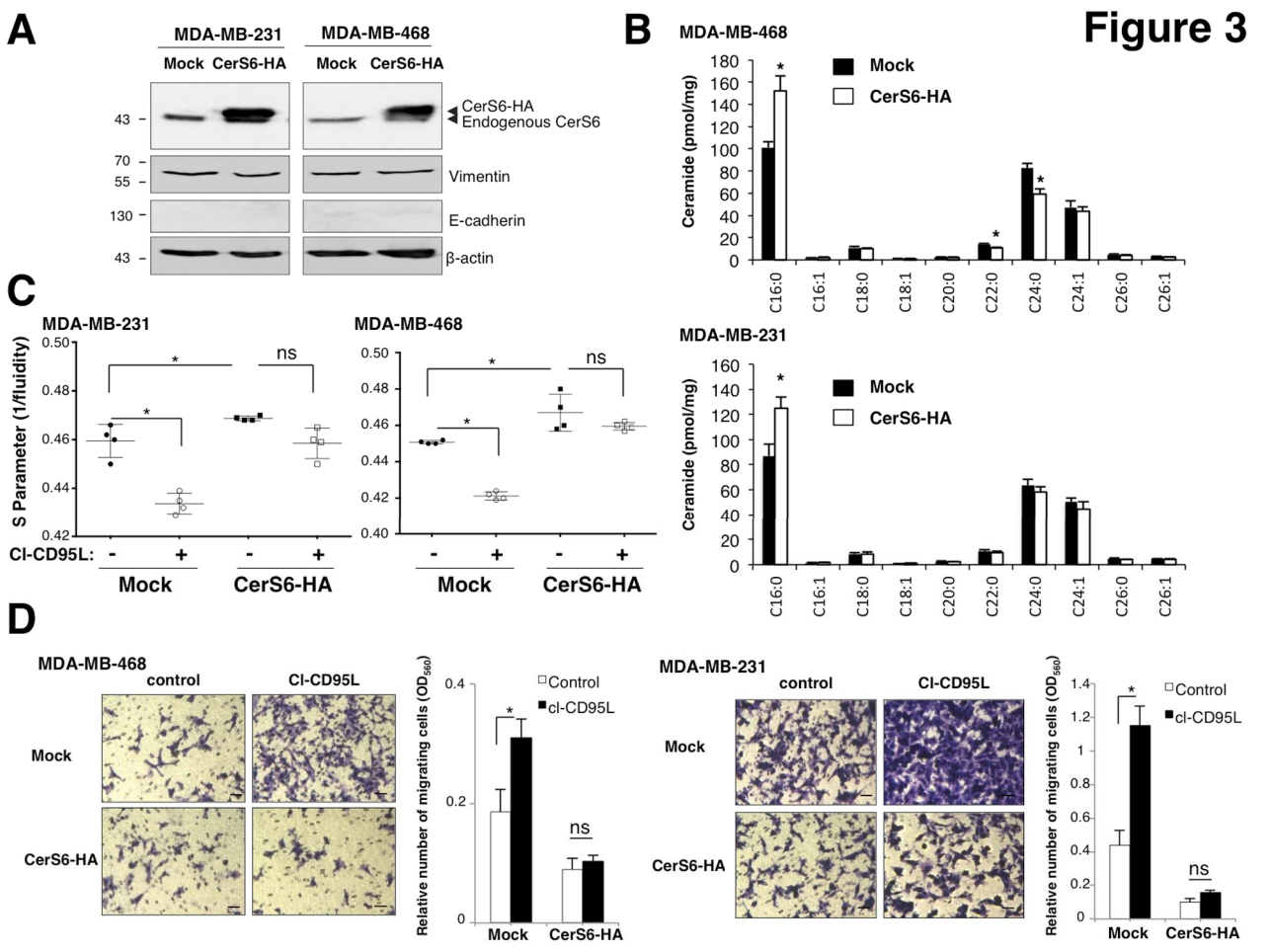
Figure 3
A
MDA-MB-231
MDA-MB-468
Mock
CerS6-HA
Mock
CerS6-HA
43
CerS6-HA
Endogenous CerS6
70
55
Vimentin
130
E-cadherin
43
β-actin
B
MDA-MB-468
Ceramide (pmol/mg)
Mock
CerS6-HA
C16:0
C16:1
C18:0
C18:1
C20:0
C22:0
C24:0
C24:1
C26:0
C26:1
MDA-MB-231
Ceramide (pmol/mg)
Mock
CerS6-HA
C16:0
C16:1
C18:0
C18:1
C20:0
C22:0
C24:0
C24:1
C26:0
C26:1
C
MDA-MB-231
MDA-MB-468
S Parameter (1/fluidity)
ns
Cl-CD95L:
Mock
CerS6-HA
Mock
CerS6-HA
D
MDA-MB-468
control
Cl-CD95L
Mock
CerS6-HA
Relative number of migrating cells (OD560)
Control
cl-CD95L
ns
Mock
CerS6-HA
MDA-MB-231
control
Cl-CD95L
Mock
CerS6-HA
Relative number of migrating cells (OD560)
Control
cl-CD95L
ns
Mock
CerS6-HA

Figure 4

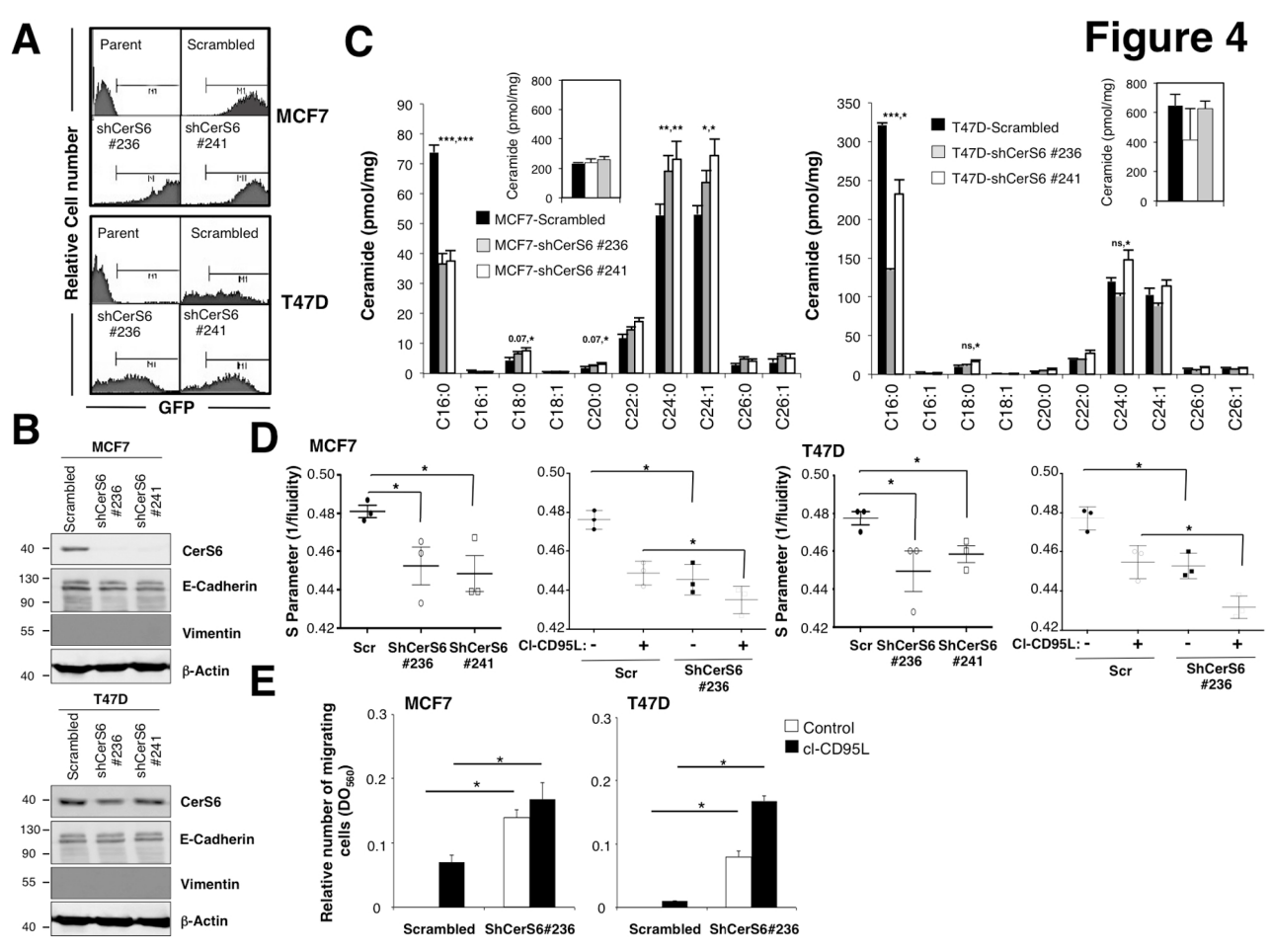
A
Parent
Scrambled
shCerS6 #236
shCerS6 #241
MCF7
T47D
Relative Cell number
GFP
B
MCF7
Scrambled
shCerS6 #236
shCerS6 #241
CerS6
E-Cadherin
Vimentin
β-Actin
T47D
C
Ceramide (pmol/mg)
MCF7-Scrambled
MCF7-shCerS6 #236
MCF7-shCerS6 #241
T47D-Scrambled
T47D-shCerS6 #236
T47D-shCerS6 #241
C16:0
C16:1
C18:0
C18:1
C20:0
C22:0
C24:0
C24:1
C26:0
C26:1
D
MCF7
T47D
S Parameter (1/fluidity)
Scr
ShCerS6 #236
ShCerS6 #241
Cl-CD95L:
E
MCF7
T47D
Relative number of migrating cells (DO560)
Control
cl-CD95L
Scrambled
ShCerS6#236

Figure 5

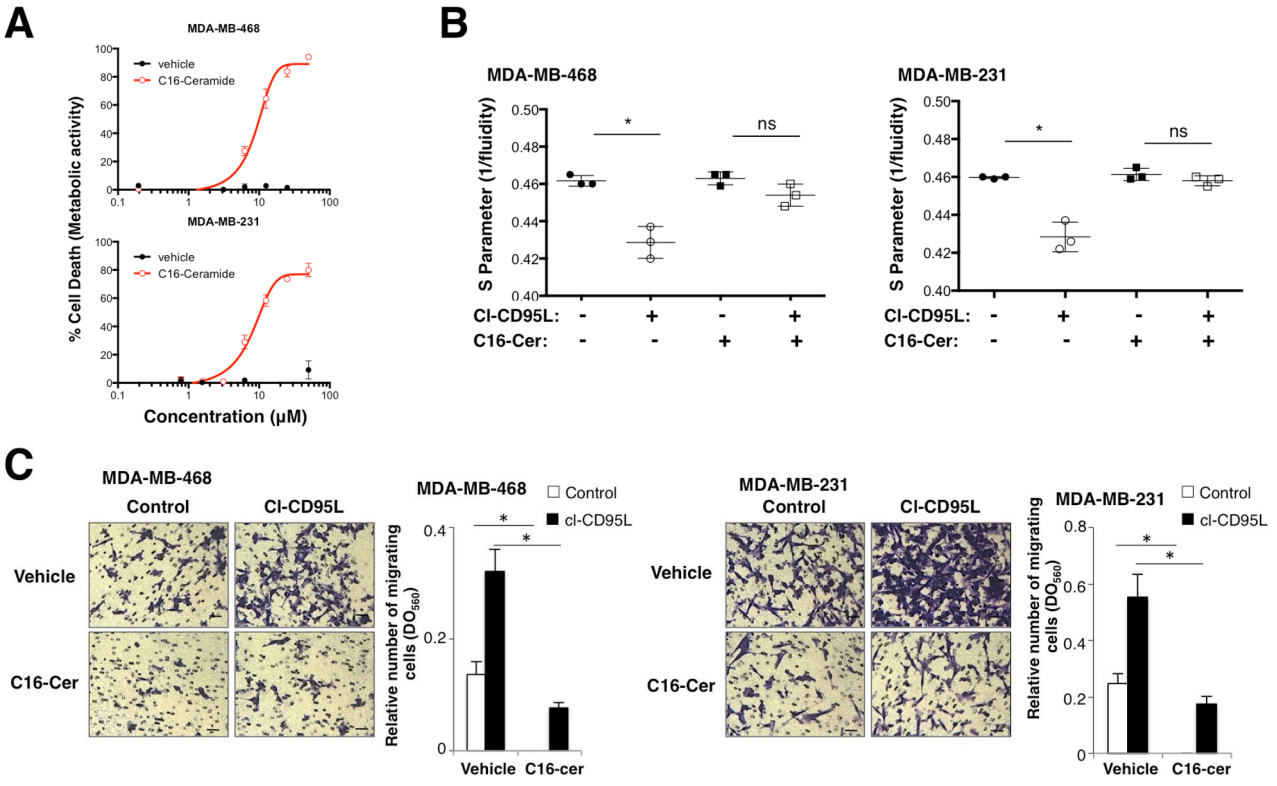
A
MDA-MB-468
vehicle
C16-Ceramide
MDA-MB-231
% Cell Death (Metabolic activity)
Concentration (μM)
B
MDA-MB-468
MDA-MB-231
S Parameter (1/fluidity)
ns
Cl-CD95L:
C16-Cer:
C
MDA-MB-468
Control
Cl-CD95L
Vehicle
C16-Cer
Control
cl-CD95L
Relative number of migrating cells (DO560)
Vehicle
C16-cer
MDA-MB-231